Turk J Pharm Sci 2024;21(6):566-576
DOI: 10.4274/tjps.galenos.2024.49768

ORIGINAL ARTICLE

In silico Evaluation of H1-Antihistamine as Potential Inhibitors of SARS-CoV-2 RNA-dependent RNA Polymerase: Repurposing Study of COVID-19 Therapy

Mazin HAMDAN[1], Necla KULABAŞ[2], İlkay KÜÇÜKGÜZEL[3]*

[1]Marmara University Institute of Health Sciences, Department of Pharmaceutical Chemistry, İstanbul, Türkiye
[2]Marmara University Faculty of Pharmacy, Department of Pharmaceutical Chemistry, İstanbul, Türkiye
[3]Fenerbahçe University Faculty of Pharmacy, Department of Pharmaceutical Chemistry, İstanbul, Türkiye

ABSTRACT

Introduction: Severe Acute Respiratory Syndrome Coronavirus 2 (SARS-CoV-2), from the family Coronaviridae, is the seventh known coronavirus to infect humans and cause acute respiratory syndrome. Although vaccination efforts have been conducted against this virus, which emerged in Wuhan, China, in December 2019 and has spread rapidly around the world, the lack of an Food and Drug Administration-approved antiviral agent has made drug repurposing an important approach for emergency response during the COVID-19 pandemic. The aim of this study was to investigate the potential of H1-antihistamines as antiviral agents against SARS-CoV-2 RNA-dependent RNA polymerase enzyme.

Materials and Methods: Using molecular docking techniques, we explored the interactions between H1-antihistamines and RNA-dependent RNA polymerase (RdRp), a key enzyme involved in viral replication. The three-dimensional structure of 37 H1-antihistamine molecules was drawn and their energies were minimized using Spartan 0.4. Subsequently, we conducted a docking study with Autodock Vina to assess the binding affinity of these molecules to the target site. The docking scores and conformations were then visualized using Discovery Studio.

Results: The results examined showed that the docking scores of the H1-antihistamines were between 5.0 and 8.3 kcal/mol. These findings suggested that among all the analyzed drugs, bilastine, fexofenadine, montelukast, zafirlukast, mizolastine, and rupatadine might bind with the best binding energy (< -7.0 kcal/mol) and inhibit RdRp, potentially halting the replication of the virus.

Conclusion: This study highlights the potential of H1-antihistamines in combating COVID-19 and underscores the value of computational approaches in rapid drug discovery and repurposing efforts. Finally, experimental studies are required to measure the potency of H1-antihistamines before their clinical use against COVID-19 as RdRp inhibitors.

Keywords: SARS-CoV-2, RNA-dependent RNA polymerase, molecular docking, H1-antihistamines, drug repurposing

INTRODUCTION

Infectious diseases caused by various microorganisms, including viruses, bacteria, fungi, and parasites, continue to be one of the most significant public health issues.[1] Among the most serious infection categories, RNA virus infections significantly contribute to the global index of mortality and morbidity associated with viral infections. Chronic disease caused by persistent RNA virus infections represents a significant public health concern.[2] The global population continues to combat many infectious diseases caused by these pathogens, some of which have become epidemics or pandemics.[3] The World Health Organization declared the Coronavirus Disease of 2019 (COVID-19), caused by Severe Acute Respiratory Syndrome Coronavirus 2 (SARS-CoV-2), a global public health emergency

*Correspondence: ilkay.kucukguzel@fbu.edu.tr ORCID-ID: orcid.org/0000-0002-7188-1859
Received: 31.05.2024, Accepted: 23.06.2024

on March 11, 2020, due to its extensive impact. By early May 2024, more than 7 million deaths and over 775 million infected cases had been reported.[4] The first known case of SARS-CoV-2 was identified in Wuhan, China. The virus is an RNA virus from the Coronaviridaefamily that rapidly led to a global pandemic because of its high transmissibility.[5-7] The Beta, Gamma, Delta, and Omicron variants arising from SARS-CoV-2 viral mutations have also caused significant damage to the world economy. Repurposed drugs and vaccines developed to combat the pandemic have played a crucial role in mitigating the pandemic's impact and restoring socioeconomic stability.[8]

Reuse can be achieved through high-efficiency *in vitro* analyses, *in vivo* animal investigations, and computer-aided drug discovery. Studies on the reuse of many known drugs, including antivirals, antimalarials, H1-antihistamines, antipsychotics, and anticancer agents, are available in the literature.[9-13] Although known safety profiles of approved drugs have allowed rapid progress in clinical trials, limited success has been achieved in identifying clinically effective small-molecule drugs for COVID-19 treatment.[14-16]

H1-antihistamines are a class of drugs commonly used to treat allergic reactions, such as hay fever, hives, and itching.[17] They work by blocking the action of histamine, a substance in the body that causes allergic symptoms. H1-antihistamines can be divided into two main types; first-generation and second-generation. First-generation H1-antihistamines, such as diphenhydramine and chlorpheniramine, tend to cause more drowsiness and are often used for short-term relief of symptoms. Second-generation H1-antihistamines, such as loratadine and cetirizine, require less sedation and are preferred for long-term use.[18] Traditionally recognized for their role in mitigating allergic responses by antagonizing histamine receptors, H1-antihistamines have recently attracted attention for their broader pharmacological effects, including potential antiviral properties. This paradigm shift is underpinned by advancements in computational modeling and virtual screening methodologies, which enable us to elucidate the intricate molecular interactions between H1-antihistamines and viral targets.

In a study conducted in 2021, H1-antihistamine agents such as hydroxyzine, azelastine, and diphenhydramine were reported to have *in vitro* antiviral activity against SARS-CoV-2. Moreover, it was reported that hydroxyzine exhibits antiviral activity through the mechanism of angiotensin-converting enzyme 2 inhibition, whereas azelastine and diphenhydramine exert their effects by binding to the sigma-1 receptor.[12] In another study reported by Ghahremanpour et al.,[11] it was found that azelastine has the potential to inhibit the main protease, which is a structural protein of SARS-CoV-2. Additionally, it has been reported in the literature that fexofenadine, another H1-antihistamine, has the potential to inhibit the SARS-CoV-2 helicase enzyme.[10] The interactions of H1-antihistamines with antiviral targets reported in the literature are summarized in Figure 1.

Although the body systems affected, transmission routes, and symptoms are different, there are many studies investigating similarities between the non-structural (NS3) proteins of SARS-CoV-2 and hepatitis-C virus (HCV). These studies indicate that these proteins share structural similarities as well as functional properties. Specifically, NS3 proteins include proteases and helicases that are critical in the replication process of both viruses. These similarities could guide the development of potentially effective antiviral agents against the NS3 proteins of SARS-CoV-2 and HCV. In a groundbreaking study published in 2014, Mingorance et al.[19] revealed compelling evidence of

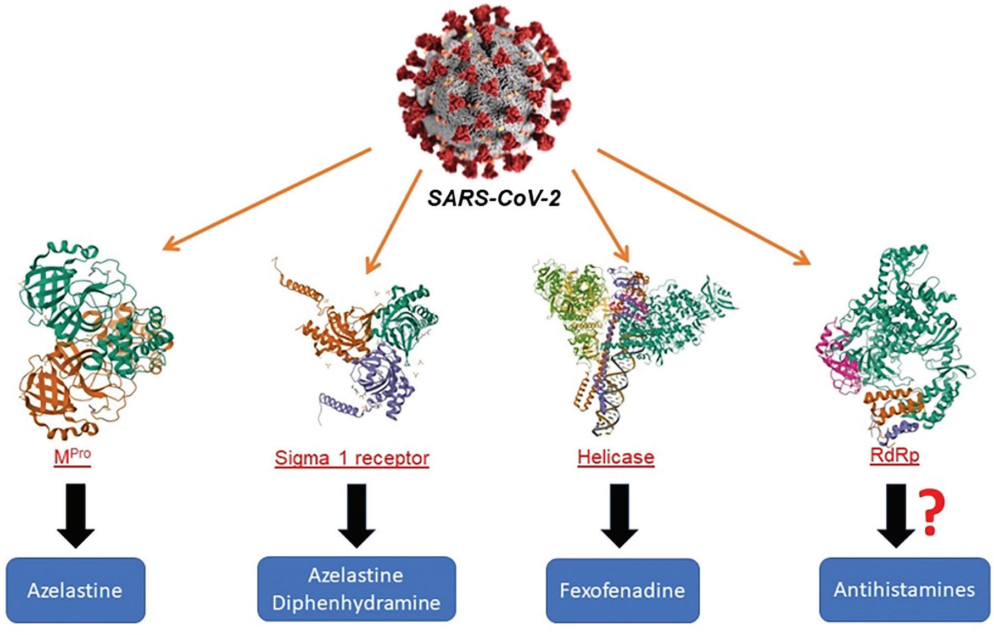

Figure 1. Antiviral effects of the known antihistamines against vital enzymes of SARS-CoV-2

SARS-CoV-2: Severe Acute Respiratory Syndrome Coronavirus 2, RdRp: RNA-dependent RNA polymerase

the selective inhibition of HCV infection by hydroxyzine and benztropine. This study, led by esteemed experts in virology, revealed the remarkable antiviral properties of these two compounds, shedding light on their potential as potent agents against HCV. Through meticulous experimentation and rigorous analysis, the researchers elucidated the mechanism by which hydroxyzine and benztropine exert their inhibitory effects on HCV infection. By selectively targeting key NS3 proteins or host cell factors crucial for viral replication, these compounds demonstrated a remarkable ability to disrupt the viral lifecycle, thereby impeding viral propagation and spread. The findings of this study not only underscore the significance of hydroxyzine and benztropine as possible candidates for antiviral therapy against HCV but also pave the way for further exploration of their therapeutic potential in combating other viral infections.[19] Similarly, a notable study by Zongyi et al.[20] revealed that chlorcyclizine exerts its antiviral effect against HCV by targeting the viral envelope glycoprotein. This finding underscores the potential of chlorcyclizine as a promising antiviral agent against HCV infection.[20]

In the dynamic landscape of drug discovery, the integration of computational techniques has revolutionized pharmaceutical intervention exploration.[21] *In silico* studies, which encompass a spectrum of computational methods, have emerged as invaluable tools for accelerating the identification and evaluation of potential drug candidates. In the approach to repurposing known drugs, the primary objective of computational and experimental techniques has been to identify existing drugs that may be effective against SARS-CoV-2.

In RNA viruses like SARS-CoV-2, the RNA-dependent RNA polymerase (RdRp) enzyme creates the machinery required for RNA synthesis and the organized replication and transcription of genomic RNA.[22] After the virus attacks a host cell, viral genomic RNA is used directly as a template, and the host cell's protein synthesis machinery is utilized to translate RdRp.[23] RdRp is an enzyme crucial for RNA virus replication.[24] It catalyzes the synthesis of RNA from an RNA template, a process essential for the reproduction of RNA viruses like influenza, hepatitis C, and coronaviruses (including SARS-CoV-2). RdRp is a prime target for antiviral drugs aimed at inhibiting viral replication. In the context of the COVID-19 pandemic, drugs like redeliver have gained attention for their ability to inhibit RdRp and potentially reduce the severity of the disease.[25] The structure of the SARS-CoV-2 RdRp complex comprises a core catalytic unit consisting of a non-structural protein 12 (nsp12) core, an nsp7-nsp8 (nsp8-1) heterodimer, and an additional nsp8 subunit (nsp8-2) (Figure 2). The nsp12-nsp7-nsp8 complex is the minimal core component of viral RNA replication.[26] The 30-kb SARS-CoV-2 genome contains 14 open reading frames (ORF) that encode at least 27 proteins.[27] The ORF 1 ab region at the 5′ end consists of a polyprotein that is hydrolyzed to 16 non-structural proteins nsp1-16 to form a replicase/transcriptase complex (RTC). The main RTC is RdRp nsp-12.[28] Nsp-12 has 8 motifs (A to G); Motif C (F753-N767) contains the catalytic motif SDD (Ser759, Asp760, and Asp761), which is required for metal-ion binding,[26] and this site is going to be our main target in this study.

This study lays the groundwork for exploring the rapidly growing field of *in silico* research aimed at uncovering the antiviral potential of H1-antihistamines. By utilizing molecular modeling techniques, we seek to understand the mechanisms behind the potential antiviral effects of SARS-CoV-2 RdRp enzyme inhibition. Moreover, these investigations provide insights into the therapeutic potential of H1-antihistamines against various viral infections, opening new possibilities for drug repurposing and therapeutic development. Although montelukast and zafirlukast are not typically classified as H1-antihistamines, they belong to a class of medications known as leukotriene receptor antagonists. These drugs work by blocking the action of leukotrienes, which are inflammatory substances produced by the body in response to allergens or other triggers. Although they are often used to manage asthma and allergic rhinitis, they do not directly target histamine receptors, as traditional H1-antihistamines do. However, they can help relieve symptoms associated with allergic reactions, such as inflammation and bronchoconstriction.[29] Since the potential of zafirlukast to inhibit the SARS-CoV-2 helicase enzyme has been reported in the literature,[30] an *in silico* investigation of montelukast and zafirlukast was also conducted.

MATERIALS AND METHODS

System preparation

Protein preparation

The recently reported high-resolution X-ray structure of RdRp (2.90 Å) (PDB ID 6M71: https://www.rcsb.org/3d-view/

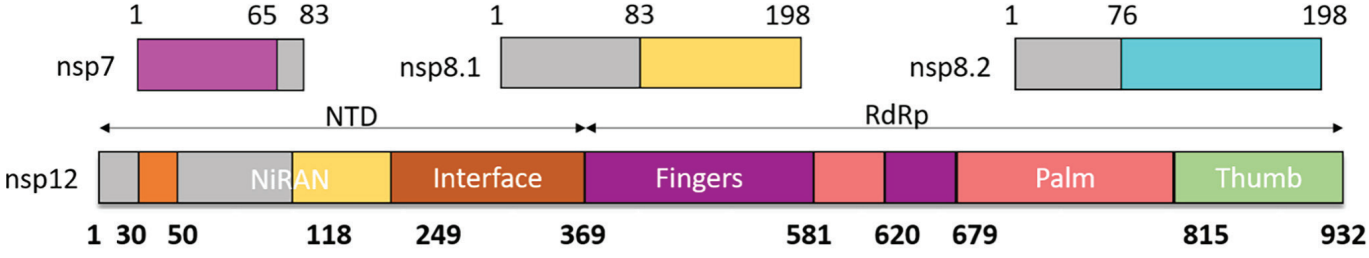

Figure 2. Domain organization of SARS-CoV-2 and its (RdRp). Interdomain boundaries are labeled with residue numbers. Here we can see nsp12[22]
SARS-CoV-2: Severe Acute Respiratory Syndrome Coronavirus 2, RdRp: RNA-dependent RNA polymerase, NTD: N-Terminal Domain

ngl/6m71)[26] was used in this study. After obtaining the protein crystal structure, all water molecules and ions were initially deleted. The protein was then saved in .pdb format and subsequently converted to .pdbqt format using Autodocktools 1.5.7.[31] Later, the regions of Ser759, Asp760, and Asp761 were determined as the locations of the grid box (114.52, 114.11,122.91) using Discovery Studio 2021 and Autodocktools 1.5.7.

Preparation of the ligands

All ligands were drawn using Spartan 4.0, and each molecule's energy was also minimized using Spartan 4.0.[32] The conformations with the lowest energy were saved in .pdb format and then converted to.pdbqt format using Autodocktools 1.5.7. Brompheniramine, levocetirizine, montelukast, and chlorpheniramine were selected as their pharmacologically active (R) stereoisomers. Cetirizine, dexchlorpheniramine, and triprolidine were selected as their pharmacologically active (S) stereoisomers.

Molecular docking

The determination of the grid box region (114.52, 114.11,122.91) and dimensions (30,30,30 Å) to include the Ser759, Asp760, and Asp761 regions was performed using AutodockTools 1.5.7. and Discovery Studio 2021. Then, molecular docking was performed using Autodock Vina.[33] Each docking process was repeated at least 3 times to ensure the accuracy of the results. Later, each molecule docking score and confirmation were visualized using Discovery Studio 2021. Each molecule's binding energy is presented in Supplementary Figure 1.

RESULTS

In this study, the *in silico* binding potentials of 37 drugs, including Food and Drug Administration-approved H1-antihistamines as well as montelukast and zafirlukast, against SARS-CoV-2 RdRp were examined (see Supplementary Figure 1). Table 1-7 present comprehensive visual representations of the three-dimensional (3D) and two-dimensional (2D) interactions of the best potential SARS-CoV-2 RdRp inhibitors, bilastine, fexofenadine, montelukast, zafirlukast, mizolastine, rupatadine, and terfenadine, respectively.

The docking results indicate that bilastine effectively binds to RdRp, primarily through hydrogen bonds and electrostatic interactions (Table 1). The strong binding energy and specific interactions suggest that bilastine inhibits the function of RdRp, potentially blocking viral replication. Bilastine showed significant binding affinity against the SARS-CoV-2 RdRp enzyme at 7.6 kcal/mol. The carboxylic acid group within bilastine forms crucial hydrogen bonds with specific residues of RdRp, highlighting the intricate nature of their molecular interactions. One notable interaction occurred between the carboxylic acid group and Asp761, wherein a hydrogen bond was established with a bond length of 2.26 Å. Additionally, another hydrogen bond was detected between this group and Ser814, further emphasizing the nuanced connectivity between bilastine and RdRp, characterized by a bond length of 2.43 Å. Moreover, the ethoxy group present in bilastine significantly contributed to its interaction with RdRp. This group forms hydrogen bonds with Asp623 and Cys622, highlighting the multifaceted nature of bilastine's engagement with the receptor. The hydrogen bond lengths between the ethoxy group and Asp623 and Cys622 were measured at 2.25 Å and 2.27 Å, respectively. Beyond hydrogen bonding, electrostatic and cationic interactions also play substantial roles in shaping the binding profile of bilastine with RdRp. The benzimidazole moiety within bilastine demonstrates such interactions with key residues of RdRp, namely Arg553 and Lys621.

These interactions occurred at distances of 4.27 Å and 4.32 Å with Arg553 and at distances of 4.94 Å and 4.78 Å with Lys621, highlighting the diverse array of molecular forces involved in bilastine-RdRp binding. The interactions with critical residues such as Asp761, Ser814, and Arg553 underscore the potential of bilastine as a therapeutic candidate and warrant further investigation.

Our docking study identified fexofenadine (Table 2) as a potential inhibitor of SARS-CoV-2 RdRp. The docking results revealed a binding energy of -8.0 kcal/mol, indicating strong binding affinity. In the context of molecular interactions, the carboxylic acid group of fexofenadine plays a crucial role by forming significant hydrogen bonds with specific residues of RdRp. Notably, hydrogen bonds were formed between Trp617 and Trp800 with bond lengths of 2.91 Å and 2.76 Å, respectively. Moreover, a particularly strong hydrogen bond was formed with Glu811, with a bond length of 2.02 Å. Beyond hydrogen bonding, fexofenadine exhibits hydrophobic and pi interactions, further enriching its binding profile with RdRp. The phenyl group of fexofenadine engages in hydrophobic and pi interactions with Tyr455 and Arg553, with distances of 5.57 Å and 4.38 Å, respectively. Additionally, multiple interactions with Lys621 were observed, including electrostatic/pi-cation interactions at distances of 4.62 Å and 5.46 Å. Furthermore, a hydrophobic/pi-alkyl interaction was noted with Arg624, at a distance of 3.09 Å. In summary, a comprehensive analysis of hydrogen bonding, hydrophobic interactions, pi interactions, and additional interactions revealed the intricate molecular landscape governing the interaction between fexofenadine and RdRp, offering valuable insights into its potential therapeutic efficacy against viral infections.

Montelukast, with a binding energy of -7.2 kcal/mol, demonstrated a multifaceted binding profile characterized by hydrogen bonding, hydrophobic interactions, and electrostatic contacts (Table 3). Specifically, the hydrogen bonds formed between montelukast and key residues Lys798, Trp800, and Asp760 underscore the importance of specific molecular recognition patterns in stabilizing the Montelukast-RdRp complex. Moreover, hydrophobic interactions with Tyr455 and electrostatic interactions with Lys621 provided additional stability to the complex, highlighting the diverse array of interactions contributing to the ligand-receptor binding. Three hydrogen bonds are predicted to form between montelukast's carboxylic acid group and residues Lys798, Trp800, and Asp760 of RdRp. These hydrogen bonds significantly contribute to the

Table 1. Interactions of bilastine with the active site of RdRp

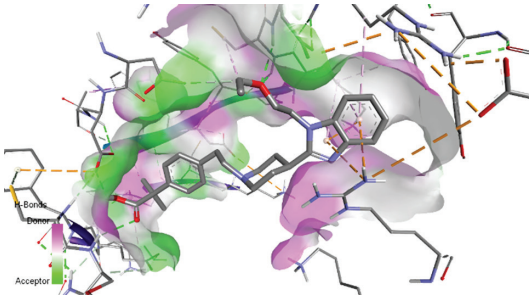

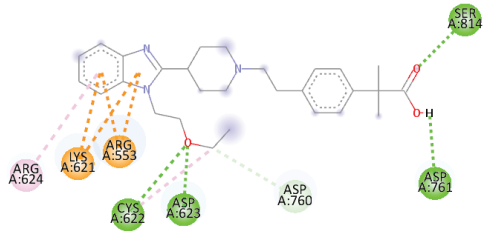

Functional group	Residue	Bond	Distance (Å)
Carboxylic acid	Asp761	H-bond (A-B)	2.26
Carboxylic acid	Ser814	H-bond (D-B)	2.43
Ethoxy	Asp623	H-bond (D-S)	2.25
Ethoxy	Cys622	H-bond (D-S)	2.27
Benzimidazole	Arg553	Electrostatic/pi-cation	4.27
Benzimidazole	Arg553	Electrostatic/pi-cation	4.32
Benzimidazole	Lys621	Electrostatic/pi-cation	4.94
Benzimidazole	Lys621	Electrostatic/pi-cation	4.78
Benzimidazole	Arg624	Hydrophobic/pi-alkyl	5.34
Ethoxy	Asp760	Carbon hydrogen bond	3.49
Ethoxy	Cys622	Hydrophobic/alkyl-alkyl	3.82

For amino acid, A: H-bond acceptor, D: H-bond donor, B: Backbone interaction, S: Sidechain interaction. Light green: Carbon hydrogen bond, Green: H-bond, Orange: Electrostatic interactions, Pink: Hydrophobic interactions, RdRp: RNA-dependent RNA polymerase

Table 2. Interactions of fexofenadine with the active site of RdRp

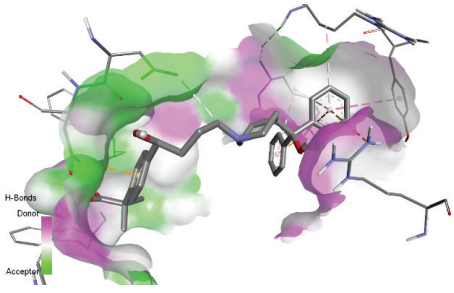

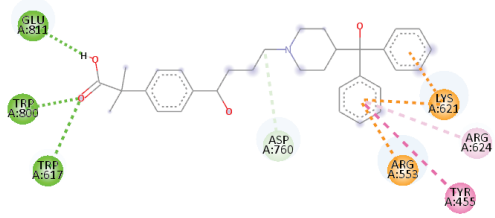

Functional group	Residue	Bond	Distance (Å)
Carboxylic acid	Trp617	H-bond (D-S)	2.91
Carboxylic acid	Trp800	H-bond (D-B)	2.76
Carboxylic acid	Glu811	H-bond (A-B)	2.02
'Phenyl	Tyr455	Hydrophobic/Pi-Pi T-form	5.57
'Phenyl	Arg553	Electrostatic/pi-cation	4.38
'Phenyl	Lys621	Electrostatic/pi-cation	4.62
'Phenyl	Arg624	Hydrophobic/pi-alkyl	3.09
''Phenyl	Lys621	Electrostatic/pi-cation	5.46
Butyl	Asp760	Carbon hydrogen bond	3.59

For amino acid, A: H-bond acceptor, D: H-bond donor, B: Backbone interaction, S: Sidechain interaction. Light green: Carbon hydrogen bond, Green: H-bond, Orange: Electrostatic interactions, Pink: Hydrophobic interactions, RdRp: RNA-dependent RNA polymerase

Table 3. Interactions of Montelukast with the active site of RdRp

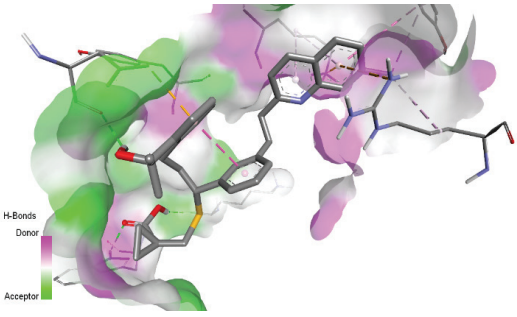

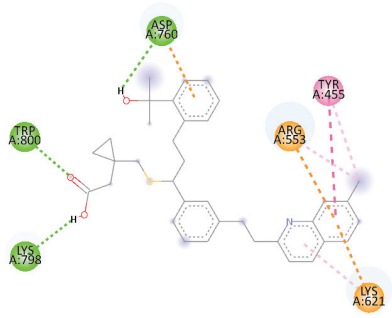

Functional group	Residue	Bond	Distance (Å)
2-Hydroxypropan-2-yl	Asp760	H-bond (A-S)	2.73
Carboxylic acid-COOH	Lys798	H-bond (A-S)	2.20
Carboxylic acid-COOH	Trp800	H-bond (D-B)	2.10
7-Methylquinoline	Tyr455	Hydrophobic/pi-alkyl	4.19
7-Methylquinoline	Tyr455	Hydrophobic/Pi-Pi T-form	5.85
7-Methylquinoline	Arg553	Hydrophobic/alkyl-alkyl	4.39
7-Methylquinoline	Arg553	Electrostatic/pi-cation	4.42
7-Methylquinoline	Lys621	Electrostatic/pi-cation	4.13
7-Methylquinoline	Lys621	Hydrophobic/pi-alkyl	4.50
4-(2-Hydroxypropan-2-yl)phenyl	Asp760	Electrostatic/pi-anion	3.25

For amino acid, A: H-bond acceptor, D: H-bond donor, B: Backbone interaction, S: Sidechain interaction. Light green: Carbon hydrogen bond, Green: H-bond, Orange: Electrostatic interactions, Pink: Hydrophobic interactions, RdRp: RNA-dependent RNA polymerase

Table 4. Interactions of zafirlukast with the active site of RdRp

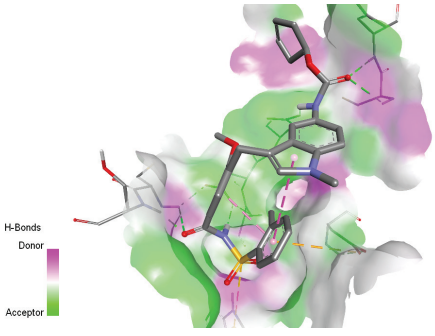

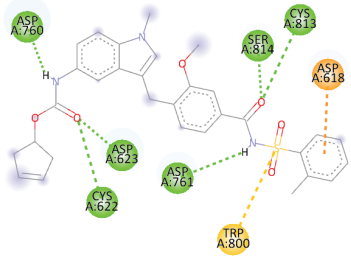

Functional group	Residue	Bond	Distance (Å)
Carbamate-NHCOO-	Cys622	H-bond (D-S)	2.61
Carbamate-NHCOO-	Asp623	H-bond (D-S)	2.24
Carbamate-NHCOO-	Asp760	H-bond (A-B)	2.29
Amide-CONH-	Asp761	H-bond (A-B)	2.06
Amide-CONH-	Cys813	H-bond (D-S)	2.91
Amide-CONH-	Ser814	H-bond (D-S)	1.83
Benzene sulfonyl	Asp618	Electrostatic/pi-anion	4.65
Benzene sulfonyl	Trp800	Pi-sulfur	4.84

For amino acid, A: H-bond acceptor, D: H-bond donor, B: Backbone interaction, S: Sidechain interaction. Light green: Carbon hydrogen bond, Green: H-bond, Orange: Electrostatic interactions, Pink: Hydrophobic interactions, RdRp: RNA-dependent RNA polymerase

Table 5. Interactions of mizolastine with the active site of RdRp

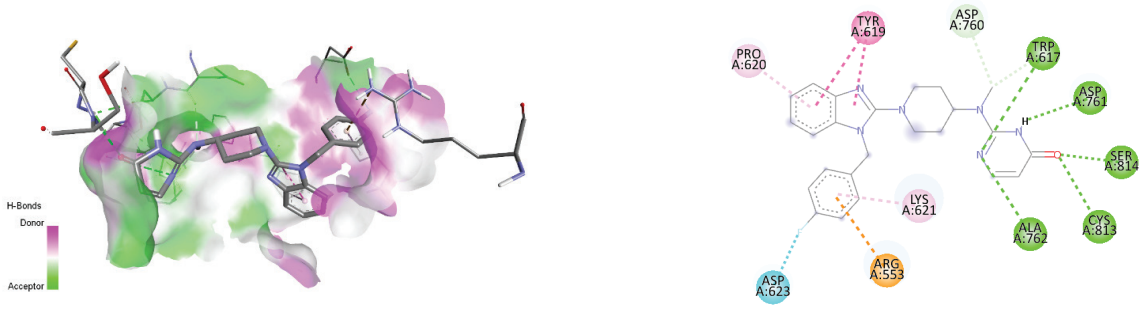

Functional group	Residue	Bond	Distance (Å)
1,3-Diazinan-2-yl	Trp617	H-bond (D-S)	3.79
1,3-Diazinan-2-yl	Ala762	H-bond (D-S)	6.58
Carbonyl	Ser814	H-bond (D-S)	2.14
Carbonyl	Gln815	H-bond (D-S)	5.74
N-methyl	Trp617	Carbon hydrogen bond	3.60
N-methyl	Asp760	Carbon hydrogen bond	3.26
Fluorophenyl	Arg553	Electrostatic/pi-cation	4.74
Fluorophenyl	Lys621	Hydrophobic/pi-alkyl	5.04
Fluorophenyl	Asp623	Halogen bond	3.15
Benzimidazole	Pro620	Hydrophobic/pi-alkyl	4.90
Benzimidazole	Tyr619	Hydrophobic/Pi-Pi T-form	4.82
Benzimidazole	Tyr619	Hydrophobic/Pi-Pi T-form	4.86

For amino acid, A: H-bond acceptor, D: H-bond donor, B: Backbone interaction, S: Sidechain interaction. Light green: Carbon hydrogen bond, Green: H-bond, Orange: Electrostatic interactions, Pink: Hydrophobic interactions, RdRp: RNA-dependent RNA polymerase

Table 6. Interactions of rupatadine with the active site of RdRp

Functional group	Residue	Bond	Distance (Å)
5-MethylPyridine	Lys621	Carbon hydrogen bond	2.89
5-MethylPyridine	Lys621	Hydrophobic/alkyl-alkyl	4.17
(5-MethylPyridin-3-yl)methyl	Tyr619	Carbon hydrogen bond	3.51
8-methyl-BenzocycloheptaPyridine	Asp761	Electrostatic/Pi-anion	3.30
8-methyl-BenzocycloheptaPyridine	Asp761	Electrostatic/Pi-anion	3.95
8-methyl-BenzocycloheptaPyridine	Trp800	Hydrophobic/pi-alkyl	4.33

Light green: Carbon hydrogen bond, Green: H-bond, Orange: Electrostatic interactions, Pink: Hydrophobic interactions, RdRp: RNA-dependent RNA polymerase

Table 7. Interactions of terfenadine with the active site of RdRp

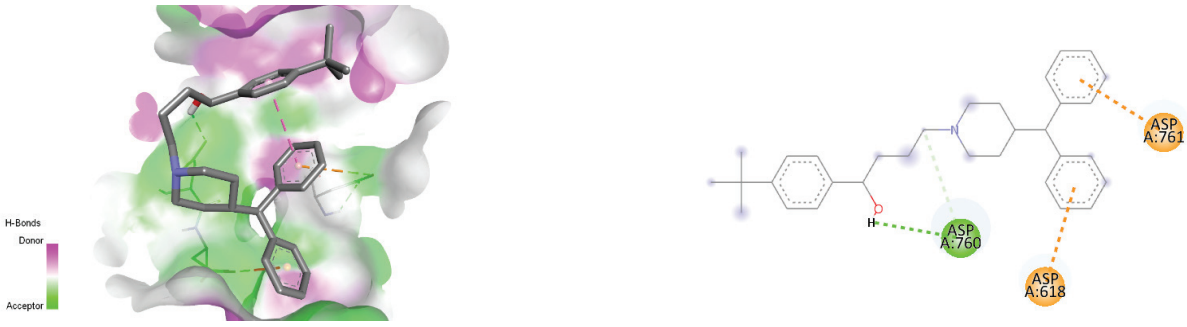

Functional group	Residue	Bond	Distance (Å)
Alcohol	Asp760	H-bond (D-B)	2.17
'Phenyl	Asp618	Electrostatic/Pi-anion	4.62
Butyl	Asp760	Carbon hydrogen bond	3.54
''Phenyl	Asp761	Electrostatic/Pi-anion	3.59

For amino acid, A: H-bond acceptor, D: H-bond donor, B: Backbone interaction, S: Sidechain interaction. Light green: Carbon hydrogen bond, Green: H-bond, Orange: Electrostatic interactions, Pink: Hydrophobic interactions, RdRp: RNA-dependent RNA polymerase

stability of the ligand-receptor complex. The 7-methylquinoline moiety of montelukast participates in many hydrophobic interactions with the Tyr455, Arg553, and Lys621 residues of RdRp, which helps retain the ligand in the binding pocket.

On the other hand, zafirlukast exhibited a higher binding energy of -8.3 kcal/mol, indicating a stronger binding affinity. The binding profile of zafirlukast was characterized by an extensive network of hydrogen bonds involving residues Cys622, Asp623, Asp760, Asp761, Cys813, and Cys814, predominantly mediated by carbamate and amide functional groups (Table 4). This intricate hydrogen bonding network underscores the specific molecular recognition events driving the formation of the zafirlukast-RdRp complex. Zafirlukast utilizes its carbamate group to form hydrogen bonds with both Cys622 and Asp623, potentially anchoring it within the binding pocket. Additionally, hydrogen bonds are formed between the ligand's nitrogens and key residues Asp760 and Asp761, potentially contributing to directional positioning. Furthermore, the participation of Cys813 and Cys814 through hydrogen bonds with the ligand's amide carbonyl group suggests a role in stabilizing the complex. The presence of a pi-anion interaction between the ligand's benzene sulfonyl group and Asp618 suggests an attractive force that could contribute to the overall binding affinity. Moreover, a pi-sulfur interaction between the same sulfonyl group and Trp800 highlights potential aromatic stacking, which further enhances the stability of the complex. The docking analysis suggests that zafirlukast binds favorably to the RdRp receptor through a combination of extensive hydrogen bonding and electrostatic interactions. These findings warrant further *in vitro* and *in vivo* studies to assess the biological significance of this interaction.

Mizolastine binds to RdRp with a binding energy of -7.6 kcal/mol, indicating a relatively strong interaction (Table 5). This interaction involves various types of non-covalent forces, including hydrogen bonds, halogen bonds, and hydrophobic interactions. Hydrogen bond interactions occurred between the 1,3-diazinan-2-yl group and Trp617 and Ala762 residues within distances of 3.79 Å and 6.58 Å, respectively. Additionally, the closest interaction with a bond distance of 2.14 Å was observed between the carbonyl and Ser814 residues. The pi-cation interaction between fluorophenyl and Arg553 was detected at a distance of 4.74 Å. While the fluoro atom was detected at a distance that could form a halogen bond with the Asp623 residue, many hydrophobic interactions were observed with the Tyr619, Pro620, and Lys621 residues.

Rupatadine interacts with RdRp with a binding energy of -7.2 kcal/mol, indicating a relatively strong binding affinity. Significant carbon-hydrogen bonds and hydrophobic and electrostatic interactions were detected between rupatadine with key residues such as Lys619, Lys621, Asp761, and Trp800 (Table 6). Hydrogen bond interactions occurred between the 5-methyl pyridine ring of Rupatadine and the Lys621 residue of RdRp. Rupatadine's 8-methyl-benzocyclohepta pyridine ring exhibited pi-anion interactions with Asp761 on RdRp. Two types of hydrophobic interactions are also observed. One occurs between the (5-methylpyridin-3-yl)methyl group of rupatadine and the Tyr619 residue of RdRp. Another hydrophobic interaction involves the 8-methyl-benzocyclohepta pyridine ring of RdRp and the Trp800 residue of RdRp.

Terfenadine interacts with RdRp with a binding energy of -7.1 kcal/mol, indicating moderate strong interaction. This interaction involves various non-covalent forces, including hydrogen bonds, electrostatic interactions, and carbon-hydrogen bonds (Table 7). An alcohol group on terfenadine forms a hydrogen bond with the Asp760 residue of RdRp at a distance of 2.17

Å. While the phenyl ring of terfenadine interacts with Asp618 of RdRp through electrostatic/pi-anion interactions, another electrostatic interaction occurs between another phenyl ring of terfenadine and Asp761 of RdRp.

The findings revealed that all seven candidate drugs exhibited superior binding energies to RdRp compared with molnupiravir, its hydrolyzed form N-hydroxycytidine (NHC), and its mono-phosphorylated (NHC-MP) derivative. This translates into a potentially stronger affinity between the drugs and the enzyme, which could be crucial for disrupting viral replication. These findings not only deepen our understanding of ligand-receptor interactions but also offer valuable guidance for rational drug design and optimization strategies for developing effective RdRp-targeting antiviral therapeutics.

DISCUSSION

The compounds with the best binding energies and poses were bilastine, fexofenadine, montelukast, zafirlukast, mizolastine, rupatadine, and terfenadine, respectively, at 7.6, 8.0, 7.2, 8.3, 7.6, 7.6, and 7.1 kcal/mol. All of these results are better than those of a previous study reported in 2021, which reported the binding energies of molnupiravir, its hydrolyzed form (NHC), and its NHC derivative (NHC-MP) at 5.7, 6.0, and -6.3 kcal/mol, respectively.[34] Higher target specificity and unique interactions of our compounds contributed to stronger binding. Extensive validation and comparison with computational data further support our findings, suggesting that these compounds offer potential therapeutic benefits.

The binding energies of azelastine, buclizine, cyproheptadine, ebastine, and loratadine were determined to be in the range of 6.9 to 6.6 kcal/mol and had better binding scores compared to molnupiravir. Cetirizine, desloratadine, hydroxyzine, levocetirizine, ketotifen, meclizine, and olopatadine exhibited similar binding scores to molnupiravir. Moreover, it was found remarkable that the seven selected H1-antihistamines exhibited strong non-covalent interactions with the amino acids Asp760 and Arg553, similar to molnupiravir and its derivatives (Figure 3). The findings revealed that all seven candidate drugs exhibited superior binding energies to RdRp compared with molnupiravir, its hydrolyzed form (NHC), and its NHC-MP. This translates into a potentially stronger affinity between the drugs and the enzyme, which could be crucial for disrupting viral replication. These findings not only deepen our understanding of ligand-receptor interactions but also offer valuable guidance for rational drug design and optimization strategies for developing effective RdRp-targeting antiviral therapeutics.

Antazoline, brompheniramine, carbinoxamine, chlorcyclizine, chlorpheniramine, clemastine, cyclizine, dexchlorpheniramine, dimenhydrinate, diphenhydramine, emedastine, promethazine, trimeprazine, tripelennamine, and triprolidine all exhibited binding energies higher than 5.7 kcal/mol. As a result, their findings were considered less significant than those of the other compounds discussed in this study. Therefore, we excluded their conformational data from this analysis.

CONCLUSION

In conclusion, the docking study conducted in this research illuminates the intricate molecular interactions between montelukast, zafirlukast, fexofenadine, bilastine, mizolastine, rupatadine, and terfenadine and the SARS-CoV-2 RdRp enzyme, shedding light on their potential as therapeutic agents against viral infections. Montelukast exhibited a binding profile characterized by hydrogen bonding, hydrophobic interactions, and electrostatic contacts with key residues of RdRp, highlighting specific molecular recognition patterns crucial for stabilizing the Montelukast-RdRp complex. Conversely, zafirlukast exhibited stronger binding affinity, engaging in an extensive network of hydrogen bonds involving multiple residues of RdRp, primarily mediated by carbamate and amide functional groups.

Additionally, electrostatic interactions further contributed to the stability and specificity of the zafirlukast-RdRp complex. Moreover, the inclusion of fexofenadine, bilastine, mizolastine, rupatadine, and terfenadine in the present study offers insights into their potential interactions with RdRp, potentially expanding the repertoire of therapeutic options against RNA viruses.

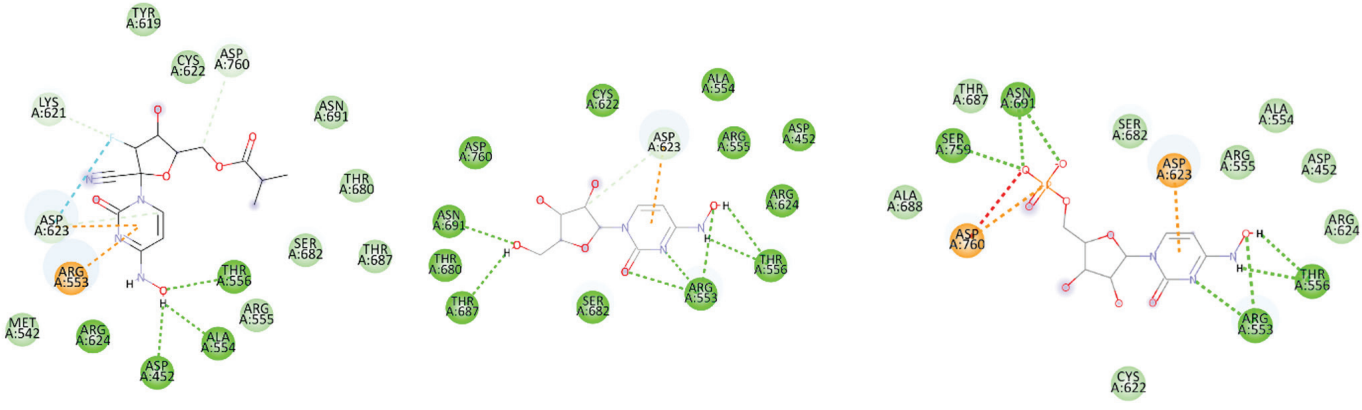

Figure 3. Molnupiravir and its derivatives in SARS-CoV-2 RdRp active site

SARS-CoV-2: Severe Acute Respiratory Syndrome Coronavirus 2, RdRp: RNA-dependent RNA polymerase

These findings provide valuable insights into the molecular mechanisms underlying the interactions between these ligands and RdRp, offering a foundation for further exploration of their antiviral potential and the development of novel therapeutic strategies targeting RNA viruses.

Ethics

Ethics Committee Approval: Not required.

Informed Consent: Not required.

Authorship Contributions

Concept: İ.K., Design: M.H., N.K., İ.K., Data Collection or Processing: M.H., N.K., Analysis or Interpretation: M.H., N.K., İ.K., Literature Search: M.H., N.K., İ.K., Writing: M.H., N.K., İ.K.

Conflict of Interest: The authors have no conflicts of interest to declare.

Financial Disclosure: The authors declared that this study received no financial support.

REFERENCES

1. World Health Organization. Infectious diseases. Available at: https://www.emro.who.int/health-topics/infectious-diseases/index.html [accessed: May 25, 2024].
2. McCarthy MK, Morrison TE. Persistent RNA virus infections: do PAMPS drive chronic disease? Curr Opin Virol. 2017;23:8-15.
3. Lee M, Kim JW, Jang B. DOVE: An infectious disease outbreak statistics visualization system. IEEE Access. 2018;6:47206-47216.
4. World Health Organization. Novel coronavirus disease (COVID-19) outbreak.
5. Zheng L, Zhang L, Huang J, Nandakumar KS, Liu S, Cheng K. Potential treatment methods targeting 2019-nCoV infection. Eur J Med Chem. 2020;205:112687.
6. Seliem IA, Panda SS, Girgis AS, Hassaneen HM, Shaldam MA, Ebeid AM. New quinoline-triazole conjugates: Synthesis, and antiviral properties against SARS-CoV-2. Bioorg Chem. 2021;114:105117.
7. Zhou P, Yang XL, Wang XG, Hu B, Zhang L, Zhang W, Si HR, Zhu Y, Li B, Huang CL, Chen HD, Chen J, Luo Y, Guo HD, Jiang RD, Liu MQ, Chen Y, Shen XR, Wang X, Zheng XS, Zhao K, Chen QJ, Deng F, Liu LL, Yan B, Zhan FX, Wang YY, Xiao GF, Shi ZL. A pneumonia outbreak associated with a new coronavirus of probable bat origin. Nature. 2020;579:270-273.
8. Krause R, Smolle J. Covid-19 mortality and local burden of infectious diseases: a worldwide country-by-country analysis. J Infect Public Health. 2022;15:1370-1375.
9. Drayman N, Jones KA, Azizi SA, Froggatt HM, Tan KS, Maltseva NI, Chen SH, Nicastro L, Florez CM, Thompson EA, Julian LD, Taylor GM, Melnyk JE, Guisado DA, Botten JW, Clay MD, Pollard KS, White KM, Schwartz O, Tay S, Vallett L, Moran P, Muramatsu H, Muramatsu T, Wu W, Keng WF, Evans RM, Komatsu T, Tsukamoto H, Gale M, Randall G, Tay SY, Schmid MF, Stevens RC, Young JA, Glenn JS, Tay HK. Drug repurposing screen identifies masitinib as a 3CLpro inhibitor that blocks replication of SARS-CoV-2 in vitro. bioRxiv [Preprint]. 2020;373:931-936.
10. Piplani S, Singh P, Winkler DA, Petrovsky N. Potential COVID-19 therapies from computational repurposing of drugs and natural products against the SARS-CoV-2 helicase. Int J Mol Sci. 2022;23:7704.
11. Ghahremanpour MM, Tirado-Rives J, Deshmukh M, Ippolito JA, Zhang C, Cho A, Anderson KS, Jorgensen WL. Identification of 14 known drugs as inhibitors of the main protease of SARS-CoV-2. bioRxiv [Preprint]. 2020:2020.08.28.271957.
12. Reznikov LR, Norris MH, Vashisht R, Gabizon R, Lee HR, Jung K, Sham HP, Solis AG, Cohen TS, Gavrilin MA, Tanjore H, Newton JC, Idell S, Yayanos M, Gouda N, Kolls JK, Smith DF, Horowitz JD, Carroll RJ, Banerjee R, Goldberg JB, Ahuja N, Thomas PG, Prokop JW. Identification of antiviral antihistamines for COVID-19 repurposing. Biochem Biophys Res Commun. 2021;538:173-179.
13. Oh KK, Adnan M, Cho DH. Network pharmacology study to elucidate the key targets of underlying antihistamines against COVID-19. Curr Issues Mol Biol. 2022;44:1597-1609.
14. Liu J, Cao R, Xu M, Wang X, Zhang H, Hu H, Li Y, Hu Z, Zhong W, Wang M. Hydroxychloroquine, a less toxic derivative of chloroquine, is effective in inhibiting SARS-CoV-2 infection in vitro. Cell Discov. 2020;6:16.
15. Wang M, Cao R, Zhang L, Yang X, Liu J, Xu M, Shi Z, Hu Z, Zhong W, Xiao G. Remdesivir and chloroquine effectively inhibit the recently emerged novel coronavirus (2019-nCoV) in vitro. Cell Res. 2020;30:269-271.
16. Dyall J, Gross R, Kindrachuk J, Johnson RF, Olinger GG, Hensley LE, Frieman MB, Jahrling PB, Laidlaw M, Kawaoka Y, Yamada M, Blaney JE, Fenton KA, Holbrook MR. Middle East respiratory syndrome and severe acute respiratory syndrome: current therapeutic options and potential targets for novel therapies. Drugs. 2017;77:1935-1966.
17. Simons FE. Advances in H1-antihistamines. N Engl J Med. 2004;351:2203-2217.
18. Church MK. Allergy, histamine and antihistamines. Handb Exp Pharmacol. 2017;241:321-331.
19. Mingorance L, Friesland M, Coto-Llerena M, Pérez-del-Pulgar S, Boix L, López-Oliva J M, Bruix J, Forns X, Gastaminza P. Selective inhibition of hepatitis C virus infection by hydroxyzine and benztropine. Antimicrob Agents Chemother. 2014;58: 3451-3460.
20. Zongyi H, Adam R, Xin H, Xiaolin H, Dalia P, Zhong L, Yuyang G, Andrew WK, Wei J. Chlorcyclizine inhibits viral fusion of hepatitis C virus entry by directly targeting HCV envelope glycoprotein 1. Cell Chem Biol. 2020;27:780-792.
21. Kitchen DB, Decornez H, Furr JR, Bajorath J. Docking and scoring in virtual screening for drug discovery: methods and applications. Nat Rev Drug Discov. 2004;3:935-949.
22. Tian L, Qiang T, Liang C, Ren X, Jia M, Yang J, Ren Y, Shen L, Wei J. RNA-dependent RNA polymerase (RdRp) inhibitors: The current landscape and repurposing for the COVID-19 pandemic. Eur J Med Chem. 2021;213:113201.
23. de Farias ST, Dos Santos Junior AP, Rêgo TG, José MV. Origin and evolution of RNA-dependent RNA polymerase. Front Genet. 2017;8:125.
24. Kirchdoerfer RN, Ward AB. Structure of the SARS-CoV nsp12 polymerase bound to nsp7 and nsp8 co-factors. Nat Commun. 2019;10:2342.
25. Elfiky AA. Ribavirin, Remdesivir, Sofosbuvir, Galidesivir, and Tenofovir against SARS-CoV-2 RNA dependent RNA polymerase (RdRp): A molecular docking study. Life Sci. 2020;253:117592.
26. Gao Y, Yan L, Huang Y, Liu F, Zhao Y, Cao L, Wang T, Sun Q, Ming Z, Zhang L, Ge J, Zheng L, Zhang Y, Wang Q, Rao Z, Lou Z. Structure of the RNA-dependent RNA polymerase from COVID-19 virus. Science. 2020;368:779-782.

27. Hillen HS, Kokic G, Farnung L, Dienemann C, Tegunov D, Cramer P. Structure of replicating SARS-CoV-2 polymerase. Nature. 2020;584:154-156.

28. Lung J, Lin YS, Yang YH, Chou YL, Shu LH, Cheng YC, Liu HT, Wu CY. The potential chemical structure of anti-SARS-CoV-2 RNA-dependent RNA polymerase. J Med Virol. 2020;92:693-697.

29. Choi J, Azmat CE. Leukotriene Receptor Antagonists. 2023 Jun 4. In: StatPearls [Internet]. Treasure Island (FL): StatPearls Publishing; 2024.

30. Al Ghobain M, Rebh F, Saad A, Alhuraiji A, Zahrani AM, Alhaddad B. The efficacy of Zafirlukast as a SARS-CoV-2 helicase inhibitor in adult patients with moderate COVID-19 Pneumonia (pilot randomized clinical trial). J Infect Public Health. 2022;15:1546-1550.

31. Morris GM, Huey R, Lindstrom W, Sanner MF, Belew RK, Goodsell DS, Olson AJ. Software news and updates gabedit-a graphical user interface for computational chemistry softwares. J Comput Chem. 2009;30:174-182.

32. Stewart JJ. Optimization of parameters for semiempirical methods V: modification of NDDO approximations and application to 70 elements. J Mol Model. 2007;13:1173-1213.

33. Trott O, Olson AJ. AutoDock Vina: improving the speed and accuracy of docking with a new scoring function, efficient optimization, and multithreading. J Comput Chem. 2010;31:455-461.

34. Kulabaş N, Yeşil T, Küçükgüzel İ. Evaluation of molnupiravir analogues as novel coronavirus (SARS-CoV-2) RNA-dependent RNA polymerase (RdRp) inhibitors-an in silico docking and ADMET simulation study. J Res Pharm. 2021;25:967-981.

Click the link to access Supplementary Figure 1: https://l24.im/CjOSE